A wave-resolving modeling study of rip current variability, rip hazard, and swimmer escape strategies on an embayed beach

Ye Yuan[1,2], Huaiwei Yang[1,2,*], Fujiang Yu[1,2], Yi Gao[1,2], Benxia Li[1,2], and Chuang Xing[1]

[1]National Marine Environmental Forecasting Center of China, Beijing, 100081, China
[2]Key Laboratory of Research on Marine Hazards Forecasting, Ministry of Natural Resources of China, Beijing, 100081, China

Correspondence: Huaiwei Yang (yanghw@nmefc.cn)

Abstract.

Drownings due to rip currents are a major threat to beach safety. In this study a high-resolution Boussinesq model with a modified wave-resolving Lagrangian tracking module has been applied to a 2-km-long embayed beach, Dadonghai of Sanya, Hainan Island, with the purpose to study rip current variability, real-time rip hazard identification, and the optimal swimmer escape strategies. Beach stage evolves periodically in the study site, and plays an important role in the long-term modulation of occurrence and strength of rip currents according to the modeling. A series of tests are designed and confirm that rip current strength is closely related to wave properties and tidal levels. Spectral analysis of output time series at specific points shows that the modeled rip currents fluctuate on the orders of 1 min and 10 min, which suggests the effects of wave-group-forced Infragravity (IG) and Very Low Frequency (VLF) motions. Rip Hazard Levels are defined by combining rip strength and its duration. An attempt of using the GPU-accelerated FUNWAVE-TVD embedded with the spectral wave model (WAM6-GPU) exhibits its capability to evaluate Rip Hazard Levels in real-time. One of the differences of the present study from the previous works is that the random, wave-resolving tracking of virtual swimmers is performed with 1-m resolution to study beach-safety strategies. The results demonstrate that multiple factors contributing to the survival of swimmers caught in the rip currents, include surf-zone bathymetry, rip strength, fine-scale flow patterns, bather's position and swimming ability. For weak-to-moderate rip currents and longshore currents, *swim onshore* consistently seems the most successful strategy across all the scenarios in this study. Higher surf-zone exit rate along the Dadonghai Beach are not favorable to *stay afloat* action, which put swimmers at a higher risk of being expelled to deeper water. The effects of wave randomness of incoming wave trains and assignment of wave-following coefficient on Lagrangian tracking are also discussed.

1 Introduction

Rip currents are narrow jets of offshore-directed flow that originated in the surf zone. Strong rip currents can reach above speeds of 0.5 - 1.0 m/s and persist for minutes, thus taking swimmers of all ability levels into deeper water (Dalrymple et al., 2011; Castelle et al., 2016b). It is reported that the majority of the bather drowning and beach rescue efforts worldwide are related to rip currents (Brighton et al., 2013; Arun Kumar and Prasad, 2014; Brewster et al., 2019; Castelle et al., 2020). In China, concerns on rip hazard was raised until recently as more coastal fatalities were reported (Li, 2016; Zhang et al., 2021).

Taking Dadonghai Beach, Hainan Island as an example, more than one hundred rescues and 7 deaths have been recorded in less than a month from August 1 to 23, 2013, according to online report (Li and Zhu, 2018). Therefore, better understanding on rip hazard is necessary for educating the public to avoid rip current-related drownings.

Wave breaking is the main driving force in surf-zone hydrodynamics by constantly producing onshore momentum and mass fluxes. Momentum and mass conservation is kept to balance these fluxes by introducing change in the mean water level near the shoreline, which provides a hydrostatic force, or a bottom friction force, due to wave-induced currents (Shepard, 1936; Bowen, 1969). It is widely accepted that rip currents are generated by alongshore variations on breaking wave heights. In the bar-trough beach, an idealized rip current system is depicted as feeder currents, rip neck, exit flow, and rip head (MacMahan et al., 2006). Incident waves break over the sandbars, and result in the formation of longshore feeder currents usually flowing along or behind the sandbar. The feeder currents converge into a narrow and fast-flowing rip neck, and then exit through incised rip channels.

The nearshore circulation is temporally unstable and spatially variable, which makes the accurate identification and modeling of rip current hazard a difficult task. Temporal variations induced by the changes in the incident wave conditions, tidal modulation, Very Low Frequency (VLF) motions, and infragravity motions, all contribute to the dynamic signature of the rip-current circulations (Reniers et al., 2010). Observations and modeling studies suggest increasing rip strength under higher wave forcing and lower tidal levels (Castelle et al., 2020). Oblique incident waves are inclined to generate strong alongshore currents, which deflects to offshore direction by headland or rigid boundary. Rip currents also pulsate at lower frequency as response to incident wave groups. The shape of the morphology (i.e., orientation, width, and rip spacing) also determines the rip current patterns, scales and magnitude (Dalrymple et al., 2011). The modeling of the localised features require fine resolution of up to 1 meter, which used to be limited by computing power.

It is important to relate knowledge on rip current dynamics with rip hazard mitigation activities. To reduce rip current hazards and keep beach safety, a series of concerns need to be addressed: how and what level of the rip hazard is in a specific beach, and how swimmers caught in a rip should react to survive. There are multiple ways to quantify or forecast rip current hazard. For bathymetrically controlled rip currents, its hazard can be inferred based on the beach morphodynamic state model proposed by Masselink and Short (1993). However, as rip currents can be present during all the evolving beach stages, meteorological and hydrodynamic factors should be included. By establishing empirical relationship among rip-related rescues, weather, wave condition, tidal level and other factors (Engle et al., 2002; Dusek and Seim, 2013), rip hazard levels can be indirectly predicted for specific beach. Since the method is empirically based, derivation of a universal relation is questionable and its validity need to be calibrated individually. Recently, the framework of predicting rip hazard by numerical tools has been proposed and implemented in Korea (Kim et al., 2013; Eom et al., 2014). With the aid of High-Performance Computation (HPC) and GPU acceleration, high-resolution beach-scale modeling of wave-driven currents are practicable using meteorological and spectral wave forecasting as forcing conditions, and thus provide a promising way to assess real-time rip current hazard in a specific region (Yuan et al., 2020).

Another category of studies focuses on field and modeling studies of the optimum current escape strategies. Field studies require the participation of experienced swimmers capable of implementing different swimming strategies as instructed. Three

typical swimming strategies tested in these studies are *stay afloat*, *swim parallel*, and *swim onshore*. Field tests organized by McCarroll et al. (2014) and Van Leeuwen et al. (2016) found that there were not versatile escaping strategy for swimmers caught in the rip currents, as significant variations in environmental factors (i.e., beach morphology, wave conditions) and resulting rip current flow regimes exist. McCarroll et al. (2015) packed a swimmer tracking and safety evaluation module to the nearshore hydrodynamic model XBEACH-SB based on depth-averaged shallow water equations. Though XBeach-SB is a phase-averaged surfzone model, it offers an additional advantage compared to other phase-averaged models in its ability to resolve wave-group generated infragravity (IG) motions, vortical currents at VLF timescales. By seeding a number of swimmers in a single rip current system, a series of scenarios and sensitivity tests are implemented to seek a preferable escape strategy. The results showed that low-speed and continuous swimming may be more effective than floating, while the choice of the best swimming direction is closely related to the starting position, rip spacing and more complex factors. Similar research has been conducted by Castelle et al. (2016a) on multiple rip channels along an open beach in France. Simulations showed that subtle changes in the bar-rip morphology had a large impact on the rip flow field, and in turn on the alongshore variability of the optimal rip current escape strategy.

To date, most of rip hazard simulations have been performed by time-averaging the phase of gravity waves. Due to the episodic and non-stationary nature of rip current flows, phase-resolving models, also known as Boussinesq-type model (BTM), are more preferable to study rip currents dynamics, and capture random, instantaneous trajectories of swimmers (Castelle et al., 2016a). In the study, a phase-resolving BTM accelerated by GPU, FUNWAVE-GPU (Shi et al., 2012; Yuan et al., 2020), is used to explore rip current variability, rip hazard and swimmer escaping strategies at Dadonghai, an embayed sandy beach with irregular rip channels at Sanya, Hainan Island. A four-grade fine-scale rip hazard map based on the numerical assessment of rip-current strength and duration is presented. The swimmer tracking and safety evaluation module proposed by McCarroll et al. (2015) is coupled to FUNWAVE-GPU to explore the swimming escape strategies. The study is a part of ongoing efforts to construct rip hazard forecasting and mitigation system for rip-prone beaches in China.

The paper is organized as follows. Section 2 provides an introduction on study site in terms of hydrodynamic background and beach morphology. In Section 3, numerical approaches on rip hazard grading and swimmer escape strategies are briefly described. The results are presented in Section 4, and further discussed in Section 5. Conclusions are made in Section 6.

2   Study site

The study site is the Dadonghai Beach, which is a medium-energy, micro-tidal, embayed beach in the south tip of Sanya, Hainan Island (Fig. 1). Generally, Dadonghai exhibits a mixed semi-diurnal tidal cycle, with an averaged micro-tidal range of 1.2 m throughout the year. The beach faces south with a horizontal span of roughly 2 km. The west end of the bay is shallow and has a coastal coral reef beneath the surface, while the east end is characterized by bedrock covered with a mixture of cobbles and boulders, suggesting high wave-energy environment. Tourists flock to Dadonghai due to its preferable climate and clear sand throughout the year, and most of them are from inland China and foreign countries. The daily tourist reception

reaches more than 5,000 per day during the peak period. The study site was selected as it is marked as a high-risk beach with rip drownings reported annually.

2.1 Surf-zone bathymetry

Two satellite images were acquired from Google Earth Historical Database on August 7, 2018 and December 26, 2019 when sea state was calm. The images feature a typically complex beach planform composed of crescentic/transverse bars and rip channels with irregular configurations. A mild slope with straight and parallel contours exists seaward of the surf zone. As highlighted in Fig. 1b-e, two sets of the surf-zone bathymetry suggest slightly different beach stages. The former exhibits shore-connected transverse sandbar with incised rip channels. White foam corresponding to breaking waves highlights the presence of shallow bars, and darker areas represent deeper rip channels that penetrate through the bars. While in the subsequent image collected in 2019, the rhythmic crescentic bar with wider yet shallower rips can be observed. Compared with the former morphology, it is supposed to generate weaker rip currents (Wright and Short, 1984).

Compared to extensive sonar or in-situ measurements of depth, shallow bathymetry can be fast and cost-effectively evaluated by remote-sensing images. In this study, by establishing a site-specific linear relationship between pixel colors and depths, nearshore bathymetry at Dadonghai was mapped and interpolated to 1-meter resolution. Although this inversion may not produce bathymetry as accurate as other approaches, it can be operationalized for rip hazard forecast in future owing to its simplicity to locate sandbars and shoals, as well as availability of satellite imagery (Radermacher et al., 2018). It should be noted that the in-situ echosounder survey was not performed in August 2018 and December 2019 for this study. For main body of the Dadonghai Bay, the depth data for the color-depth correlation was from nautical chart published by China Navigation Press with a scale of 1:25000, which was converted to the mean tidal level (MTL) based on the datum at Sanya Tidal gauge nearby. Surf-zone bathymetry is constantly changing in multiple temporal scales. For the surf zone that is not covered by the nautical chart, only very limited field data collected in October 2019 was available to derive the color-depth relation along the surf zone. The derived bathymetry was then rotated 90 degrees to align the shoreline with the vertical axis. The rotation is necessary for FUNWAVE to apply irregular wave maker.

2.2 Wave conditions

Based on an analysis of 30-year wave hindcast dataset developed by the National Marine Environmental Forecasting Center of China (NMEFC), wave conditions immediately off the Dadonghai Bay are assessed. The wave point for analysis is located at 109.5° E, 18.2° N, which is denoted as a yellow triangle in Fig. 1a. According to wave rose diagram of 30-year-long wave hindcast (Fig. 2a), generally the Dadonghai Bay receives waves at two prevailing directions, including powerful typhoon swells mainly from the south, and monsoon swells from the southeast. The 1-day moving average on the hourly wave hindcast in 2018 is performed and shown in Fig. 2d for further analysis. Waves during the summer months are relatively more energetic than in winter immediately off the Dadonghai Bay, which is interspersed with high-energy events associated with typhoon activities in the northern South China Sea (SCS). Typhoons can send long-period swells to the Dadonghai Bay. Wave-buoy observations along the slope of the Northern SCS demonstrate that while peak wave period during the winter monsoon is between 4 - 8 s, it

125   is capable to reach up to 10 - 14 s during the passage of the tropical cyclones in summer (Xu et al., 2017; Tian et al., 2020). As shown in Fig. 2c, these storm waves arrive over a wide spread of directions from SE to SW. As typhoons enter the northern SCS and move west, the directions of waves receive by the Dadonghai Bay vary over time. Two prominent peaks in July and August are explained by two typhoons moving westward through the Northern SCS in 2018 summer, leading to elevated significant wave height of 1.5 - 2.5 and 2.0 - 4.0 m (without 1-day moving average), respectively. Strong typhoon swells persist for a

130 week. During the winter months, the prevailing winter monsoon constantly produce northeast wind waves in the Northern SCS with significant wave height of more than 2 - 3 m. However, as the monsoon swells propagate into the bay from the open sea, the waves get weaker in wave height and are diffracted to the southeast due to shelter of the peninsula to the east (Fig. 2b). The hourly significant wave height off the Dadonghai Bay generally varies below 1.0 m, and can reach up to 2.0 m with the outbreak of monsoon.

135   Accordingly, various wave conditions representative of winter monsoon swells and summer typhoon swells are used in the following modeling studies of rip variability.

3   Methods

3.1   Numerical model

Phase-resolving Boussinesq-type wave models have proven to be robust tools for modeling surface waves and wave-driven

140 processes in the nearshore region (Shi et al., 2012; Chen et al., 1999, 2003; Geiman et al., 2011). In this paper, we use the FUNWAVE-TVD (total variation diminishing version of the fully nonlinear Boussinesq wave model) to simulate rip current dynamics. Due to the existence of high-order dispersive terms, FUNWAVE-TVD is more computationally demanding compared with shallow water equation solvers (Kirby, 2016). To address this problem, a multi-GPU-accelerated version of FUNWAVE-TVD (FUNWAVE-GPU) has been developed recently (Yuan et al., 2020).

145   In this study, random, directionally incident waves are generated, propagate shoreward, and then shoal, break, finally produce wave setup in the surf zone. The computation domain is 1678×659 m^2. The cross-shore and alongshore grid size is chosen to be 1 m with variable time step determined by Courant–Friedrichs–Lewy (CFL) stability condition. The fine resolution is required to resolve wave-induced flow behavior with different scales. In the study time step is usually smaller than 0.04 s, which is necessary to resolve individual wave. A constant bottom drag coefficient of 0.0025 in the quadratic friction formula was applied

150 (Zhang et al., 2022). The directional irregular wavemaker is placed at 10-m water depth offshore, which is approximately 500 m away from the shoreline. The wavemaker can generate random, normally or obliquely incident waves with specified peak amplitude, period and incident angle. The absorbing boundary conditions are placed behind the wavemaker. The offshore sponge layer has a width of 100 m and is used to absorb outward-propagating waves. Wave breaking is modeled by two schemes implemented in the FUNWAVE; either the shock-capturing scheme of Tonelli and Petti (2009), or the eddy-viscosity

155 scheme following Kennedy et al. (2000). The latter scheme is used in the study. The wave-driven flow field is obtained by averaging the instantaneous fluid particle velocity over two wave periods.

Table 1. Model input for sensitivity tests (T1-T9) of rip currents on incident wave conditions and tidal levels.

Tests	H_{peak} (m)	T_{peak} (s)	λ (°)	Tide (m)
T1	0.7	12.0	0	0
T2	1.0	12.0	0	0
T3	1.3	12.0	0	0
T4	1.8	12.0	0	0
T5	1.0	4.5	0	0
T6	1.0	8.0	0	0
T7	1.0	12.0	5	0
T8	1.0	12.0	20	0
T9	1.0	12.0	0	+0.6

Besides, unlike previous studies on rip current dynamics and bather tracking using wave-averaging models with coarser grid resolution, this study provides a chance to showcase to what extent the tracking can be different with wave-resolving and wave-averaged flow velocities, respectively.

3.2 Hydrodynamic settings

Prediction of nearshore circulation is important for swimmer safety and for estimating surf-zone dispersion of sediments and pollutants. Rip currents are forced by incoming waves, and modulated by tidal elevation and other low-frequency motions MacMahan et al. (2006). In the study, the hydrodynamic response of rip currents is examined by a series of numerical tests with varying offshore wave forcing conditions and tidal elevations. Shallow bathymetry within the surf zone largely dictates where incident waves break, thus two sets of bathymetry shown in Fig. 1b-e are also applied. In each simulation, the model runs for 50 min, with the first 10 min neglected due to a cold startup.

Model input is summarized in Tab. 1. The peak significant wave height and period range from 0.7 m to 1.8 m and from 4.5 s to 12.0 s, respectively. The incident angle varies from shore-normal direction (0°) to obliquely incident (20°). Tidal elevation is considered by adjusting input bathymetry according to averaged tidal range at the Dadonghai Beach. Wave conditions given in these 9 tests are representative of summer typhoon swells and winter monsoon swells, and hereafter referred to as T1 - T9.

3.3 Rip Hazard Levels

In this study the rip currents are defined as the offshore-directed flow with direction values falling between 135 and 225° clockwise from North. The rip strength is divided into 4 intervals shown in header row of Tab. 2. For each rip strength interval, its duration is the accumulated time period (t_{rip}) when the velocity falls into it during the entire simulation period ($t_{modeling}$). Rip duration is simply measured by $t_{rip}/t_{modeling}$, and categorized as 4 levels listed in the first column of Tab. 2. To quantify

Table 2. Classification of rip hazard based on the rip strength (m/s) and rip duration ($\frac{t_{rip}}{t_{modeling}}$).

Rip duration ($\frac{t_{rip}}{t_{modeling}}$)	Rip strength (m/s)			
	$V_{max} < 0.3$	$0.3 \leq V_{max} < 0.6$	$0.6 \leq V_{max} < 0.9$	$V_{max} \geq 0.9$
$0.05 \leq t_{rip}/t_{modeling} < 0.1$	1	2	3	4
$0.1 \leq t_{rip}/t_{modeling} < 0.2$	2	4	6	9
$0.2 \leq t_{rip}/t_{modeling} < 0.4$	3	6	9	12
$t_{rip}/t_{modeling} \geq 0.4$	4	8	12	16

Rip Hazard Level: Grade IV $\in$ [1,4]; Grade III $\in$ [5,8]; Grade II $\in$ [9,12]; Grade I $\in$ [13,16]

rip hazard, here we propose the term of Rip Hazard Level, and define it as a combination of rip strength and duration. The classification is summarized in Tab. 2. Grade I denotes the highest Rip Hazard Level potentially posing the greatest danger to the bathers, and Grade IV is the lowest. Rip Hazard Levels are evaluated at locations where the water depth is deeper than 0.8 m. Below this depth, it is assumed that an adult of average height is capable of standing firmly in the water even with high-energy wave condition.

3.4 Phase-resolving tracking of swimmers and safety criterion

The existing Lagrangian tracking module of FUNWAVE has been modified to simulate the movement of swimmers with a combination of instantaneous, random wave motion ($\tilde{u}_w$) and swimming velocity (U_s), as shown in Eq. 1. The effect of individual wave on swimmers can be resolved due to the phase-resolving nature of Boussinesq type wave model. Swimmers are initially seeded as particles in the surf zone with the wave orbital motion and the mean depth interpolated from the neighboring four grid points at each time step $\triangle t$. Each particle is also assigned with a fixed swimming velocity and direction at each $\triangle t$. c_f is defined as the wave-following factor of the swimmers, which accounts for the correction of drifting speed. In this study c_f=0.8 is adopted following previous studies (McCarroll et al., 2015; Castelle et al., 2016a). A sensitivity study of this factor is also included in Discussion.

$$u_{tracking} = c_f \tilde{u}_w + U_s. \tag{1}$$

The safety check of swimmers follows the work of McCarroll et al. (2015), which established a local hazard rating criterion HR (Eq. 2) to check whether swimmers have reached a safe state.

$$HR = \overline{d}(\overline{U} + 0.5), \tag{2}$$

where $\overline{d}$ is the mean water depth, and $\overline{U}$ is the wave-averaged flow velocity. As shown in Table 3, a successful escape should satisfy that the swimmer is at a position where either the mean water depth or the HR-value is below a threshold (d_{safe}, or HR_{safe}). The rip escape simulation is performed in the domains indicated in Fig. 1 by red rectangles. The swimmers are seeded in the rip channels uniformly with a spacing of 5 m when the modeling reaches a steady state. Although elite swimmers

Table 3. Configurations of rip escape strategies and safety check criterion

Swimming Strategies		Adult		Child	
		$U_{swim}(m/s)$	Safety check	$U_{swim}(m/s)$	Safety check
Stay afloat		0		0	
Swim onshore		0.2, 0.4	$HR_{safe} = 0.7m^2/s$	0.2	$HR_{safe} = 0.5m^2/s$
Parallel to shoreline	westward	0.2, 0.4	$d_{safe} = 1.1m$	0.2	$d_{safe} = 0.7m$
	eastward	0.2, 0.4		0.2	

can propel themselves at up to 1 m/s in still water, here we assume that the average swimmers caught in rip currents have a swimming velocity of 0.2 - 0.4 m/s. Swimmers are supposed to be exhausted, and thus removed from the subsequent simulation when a maximum time period of 10 minutes is exceeded. The escape time (t_{safe}) is recorded after each swimmer reaches the safe state. Three escape strategies, as suggested by McCarroll et al. (2015) and Castelle et al. (2016), are tested in the study, including *stay afloat*, *swim onshore*, and *swim parallel to shoreline*. For *stay afloat* strategy, U_{swim} equals to zero, suggesting swimmers completely move with ambient wave motions. Table 3 provides a summary on rip escape strategies and safety check criterion. Adult and child have different swimming capability and safe check conditions.

4 Results

4.1 Hydrodynamic response to wave conditions and surf-zone bathymetry

By applying two sets of beach morphology obtained in 2018 and 2019 in the simulations, the snapshot of nearshore circulation forced by different wave climates and tidal conditions are shown in Fig. 3-4. In Fig. 3a-d, the most prominent feature is that two opposite embayment-scale longshore currents originate from both ends of the bay with maximum flow velocity reaching 0.9 m/s. The incident waves shoal and break at both headlands immediately after entering the embayment, and in turn produce alongshore variable wave setup creating longshore currents. The presence of strong lateral shear in the cross-shore direction leads to the meandering of the longshore flow, which gradually deflects to offshore direction at x = 600 m and 1400 m. This feature is also visible in the CCTV images of the Dadonghai Beach (Fig. 9 in Li (2016) and Fig. 6 in Wang et al. (2018)) in the same location. Swimmers who caught in these mega rips may exit the surf zone rapidly. Rip current dynamic within the red rectangle is enlarged in Fig. 3e-l. The incised rip channels with uneven spacing produce complex surf-zone flow regime. Generally, rip currents get stronger with increasing incident wave height. For test case H_s = 1.0 m and T_p = 12 s, a intense shore-normal rip current (0.6 m/s) at x = 900 m is generated with stable feeder currents from neighboring sandbars. This well-established rip extends more than 150 m offshore, and persists over the entire simulation. The animation shows considerable vibration of rip direction and accompanied vortex structures.

Nearshore circulation is weaker in terms of extent and strength for incident waves with shorter period. Dadonghai Beach faces the Northern SCS. While the period of incoming waves are generally within 4-8 s, the long-period swells with period of 8-

14 s occasionally propagate into the embayment during the typhoon season. Averagely, there are more than 13 tropical cyclones (TCs) across the Northern SCS annually from early March to later November. Swells arrive days before the landing/passing of TC and usually last for more than a week. Even subtle variation in incident direction can induce considerable transition of flow pattern. Offshore-directed flows are suppressed and rapidly deflected to longshore direction.

The surf zone of sandy beaches usually shows a variety of complicated morphological patterns appearing alternatively with time. The beach morphology on December 26, 2019 exhibits a different beach stage. The satellite image (Fig. 1d-e) shows a nearly straight shore-parallel sandbar approximately 80-100 m seaward from the shoreline with periodic horn-shape bars weld to the shore, causing the discontinuity of alongshore trough between the shoreline and outer sandbar. This state is known as crescentic bar. Compared with previous beach state in 2018 (Fig. 1c-d), there is no typical rip channels which are characterized by penetrating exit openings. The presence of relatively small bathymetric variations can have a profound effect on rip circulation. In this case, weaker exit flow is expected. As shown in Fig. 4a-h, the circulation is mainly confined within the surf zone, and no persistent and well-established exit flow is formed. The animation also suggests rip flow patterns consist of semi-enclosed vortices developed within the wide channels, resulting in spatial and temporal variability in flow strength and direction. Although using Boussinesq model shows its superiority in studying fine-scale nearshore circulation and its variability in surf zones (Shi et al., 2012; Chen et al., 1999, 2003; Geiman et al., 2011; Feddersen, 2014; Zhang et al., 2022), further analysis on rip pulsation and variability in this study has not been included due to lack of field observations at the Dadonghai Beach.

We use rip-current rose diagram to interpret the temporal distribution of rip current speed and direction over the entire simulation period. The time series of rip current at Gauge A ($x = 730$ m, $y = 120$ m, Fig. 1f) is interpreted by rose diagram in Fig. 5. The length of each colored spoke is a measure of the percentage of time that the rip current flowing to that particular direction. For moderate wave energy with $H_s = 1.0$ m, the rip is nearly shore-normal with a magnitude varying between 0.3 - 0.6 m/s. The rip strength can exceed 0.6 m/s occasionally with $H_s = 1.3$ m. The wave-driven flow is weaker and shows considerable variability in direction when incoming waves have shorter period. Tidal modulation of rip current has long been confirmed by a number of observational and modeling studies (Dalrymple et al., 2011; Castelle et al., 2020). Generally rip strength is well correlated to tidal level, with maximum rip currents occurring at low tide. In Fig. 5f, by deepening the bathymetry with a constant of 0.6 m, rip current is replaced by a weak, and meandering alongshore flow regime that is coupled to the underlying surf-zone morphology.

Temporal variation of rip currents is closely related to the forcing mechanisms and local bathymetry features (Reniers et al., 2010). We placed a group of gauges at well-formed sandbars and rip channels along the shore with output interval of 2 s. The majority of gauges show periodic fluctuations on flow magnitude and direction at multiple temporal scales. Fig. 6 illustrates analysis on time series of Gauge B within a rip channel ($x = 1060$ m, $y = 105$ m of bathymetry on August 7, 2018). The rip flow exhibits intermittent, periodic nature with flow direction oscillating from side to side in the channel. Normalized power spectra of the modeled current (gray line) are plotted in subplot (b). The spectra shows a broad-banded feature, with two prominent peaks occurring at $T = 80$ - 100 s and 8 - 10 min, which correspond to period bands of infragravity pulsations and Very Low Frequency (VLF) motions, respectively. The incident wave groups have been known as main cause of rip

fluctuations at infragravity band (MacMahan et al., 2004a, b). The time series of incident wave height confirms the existence of wave group effect, and its power spectrum (dashed line in Fig. 6b) shows an energy peak at 80 - 100 s. Within an wave group, arrival of higher waves break and produce greater wave setup over bars, which results in stronger pressure gradient, and expels excess water offshore through an intensified rip flow. This effect contributes to velocity variation of 0.1 - 0.2 m/s in Gauge B. The presence of VLF motions can not be explained by wave forcing due to the absence of spectral peak at corresponding period band. By observing rose diagram and vector plot of rip flow in subplot (c-d), the VLF motions are characterized by the periodic shift of flow direction, which is usually related to the formation of vortex due to local morphology. Besides, while infragravity wave-group fluctuation is permanent for all gauges, VLF motions are only present in some of them. It is expected that swimmers in a weak rip current system at a specific time may be caught in strong flow soon afterwards due to the sporadic feature of rip currents.

4.2 Rip hazard maps

Using the rip hazard index table proposed in Section 3.3, rip hazard is interpreted quantitatively by an integration of rip strength and duration at each grid point. Therefore, Rip Hazard Levels are representative of both offshore-directed flow velocity and its persistence. In Fig. 7, spatial distribution of Rip Hazard Level is overlapped with the satellite images acquired on August 7, 2018 and December 26, 2019. Grid points with depth less than 0.8 m are masked.

As shown in Fig. 7, strong rip currents originate from the rip channels or troughs overall. A close examination of left panel finds that the area of white foam is staggered with rip necks. Rip hazard with transverse-bar morphology (Left panel) can produce higher hazard level of Grade-II. Strong rips can potentially eject swimmers seaward rapidly with the maximum extent of 100 - 200 m. Due to the existence of mega-rip originated from the deflected longshore currents at both flanks of the embayment (x = 400 and 1400 m in Fig. 3-4), the area of Grade-III rip hazard spreads more than 200 m seaward. Swimmers who are caught into the deflected longshore currents may exit the surf zone unawares.

In the study, by using the Nvidia A100 graphic card, a maximum of speedup of 8-10 fold is achievable using FUNWAVE-GPU, compared with a 36-core Intel CPU node. A modeling of beach-scale wave propagation, breaking and associated nearshore circulation can be completed within 10 min (Yuan et al., 2020). Recently the WAM6 spectral wave model (Group, 1988) has been modified and accelerated by OpenACC by the authors (WAM6-GPU, source code can be accessed upon request). The computation time for a 5-day 1/12° wave modeling of the Chinese offshore regions (0 - 45° N, and 95 - 135° E) on Nvidia A100 card is dramatically reduced to approximately 5 min. By feeding the FUNWAVE-GPU with 2D directional spectrum data obtained from the basin-scale spectral wave modeling, or simply specifying peak wave parameters and tidal levels, it is possible to generate real-time rip hazard maps with fine resolution when nearshore bathymetry is available. It is helpful for beach safety practitioners to deploy rescues appropriately.

4.3 Swimmer escape simulations

Virtual swimmers seeded in Area 1 and Area 2 with different escape strategies are traced by instantaneous, wave-resolving velocity with wave forcing condition of H_s = 1.0 m and T_p = 12 s. The modeling results are shown in Fig. 9-12. Area 1 is a

wide rip channel located between 860 m and 1000 m of the longshore axis, as marked in Fig. 1f. The water depth is slightly shallower at the seaward exit of the channel. According to Fig. 4, Area 1 does not contain a typical underlying morphology to incubate strong rip currents. The flow magnitude and direction show a large degree of variability due to the formation of a strongly asymmetric Counter-Clockwise Eddy (CCE) within the channel during the simulation, which is supposed to retain swimmers within the surf zone for a longer time. Area 2 is characterized by several parallel longshore isobaths without obvious rip cell. Stable longshore currents exist in this area, which gradually deflect to offshore direction at x = 500 - 600 m. Due to the fact that rip currents are unstable and oscillate in multiple time scales, a series of tracking simulations are conducted with virtual swimmers seeded at different model times with an interval of 150 s. As suggested by Fig. 8 , the modeled trajectories of the virtual swimmers show considerable variability when choosing different seeding times, which results in variations of escape time t_{safe} histograms accordingly. t_{safe} hereafter is an average of all simulations with different seeding times. Besides, we also selected a typical rip channel for modeling study of swimmer escape. As the conclusion was similar with the previous studies (McCarroll et al., 2015; Castelle et al., 2016a), the modeling result was not included in this manuscript.

4.3.1 Stay afloat

Swimmers adopting *stay afloat* strategy are subject to ambient current field (McCarroll et al., 2015; Castelle et al., 2016a). In Area 1, rip flow is relatively weak in strength, and oscillates in direction due to the existence of a recirculating flow regime. The majority of floaters are trapped in the eddy, with their trajectories exhibiting complex vortical patterns. Most of them eventually exit the surf zone after 10-min floating. Only a few of floaters are transported to the western sandbar within 10 min, where it is safe to stand and walk to shore for adults (Fig 9a-b). In Area 2 where the intense longshore flow is dominant due to the presence of headland with submerged coral reefs, over 90% of the floaters are swept eastward along the isobaths and eventually expelled offshore at x = 400 - 500 m (Fig. 9e-f). The swimmers who are not aware of this strong longshore jets may be gradually dragged away from the surf zone unconsciously. Generally, adult has slightly higher chance to survive than Child.

    Swimming and floating actions are two sides of the same coin when swimmers notice of being caught in a rip. Swimming against the flow may result in muscular fatigue and cramp, especially for beginners; while adopting floating strategy can save energy and increase the possibility of being rescued. For rhythmic bar-trough beaches, floating or swimming parallel are supposed to be reasonable choices, which help the swimmers escape from the rip jets and reach the proximate sandbars safely. However, according to the modeling study of Area 1 and 2, using the strategy of *stay afloat* alone is obviously an unwise action, suggested by over 90% of failure rate. The alongshore variability of underwater topography increases the complexity of flow regime. There is no versatile escape strategy even in the same beach.

4.3.2 Swim onshore

Swimming onshore is thought to be an instinct to survive from the rip currents for most of swimmers. In Area 1, 100% of skilled swimmers with onshore swimming velocity U_s = 0.4 m/s can reach safety in less than 8 min (Fig. 10b, e). The t_{safe}-value depends on the distance of swimmer to safety depth (d_{safe} = 1.1 m for adult), as well as their initial position within the surf zone. It takes longer time for swimmers seeded between x = 920 and 940 m to reach the safety depth as they need swim

against the CCE inside the trough. Any hesitation or interrupted swimming may lower the chance of survival even for skilled swimmers. The recirculating flow is hazardous for children due to their weaker swimming ability and longer distance to safety depth (d_{safe} = 0.7 m). On average, the failure rate is over 50%. Most of failures occurs at rip neck and downdrift of rip eddy. In Area 2, almost all the bathers with different swimming abilities can reach safety within a relatively short time. Obviously for bathers caught in a longshore current, swimming onshore is the best choice. Generally, adopting strategy of *swim onshore* seems quite successful. However, for swimmers caught in the offshore-directed jet of a typical rip-flow system, a combination of actions of swimming parallel and onshore should be a more optimal strategy than swimming onshore alone.

4.3.3 Swim parallel to shore

The successful rate by taking *swim parallel to shore* actions is largely subject to the specific locations of bathers and swim direction relative to the current. As shown in Fig. 11, for bathers seeded in CCE-dominated Area 1, only those within the inner surf zone can reach the downdrift sandbar and are able to stand firmly by themselves. However, some of beginning bathers or children who swim westward across the CCE are swept offshore a bit by the meandering rip current, and then fail to reach the western sandbar (Fig. 11a, c). When caught in the rip currents, the first priority is to escape from the jet as soon as possible. In Area 1, some beginning bathers who swim eastward against the flow are at greater risk of being stuck in the CCE, which is clearly observed by the circular trajectory in Fig. 12a. Though these bathers are seeded in the inner surf zone, they fail to reach safety within 10 min by choosing an inappropriate swimming direction. In Area 2 (Fig. 11g-i), the eastward longshore current is gradually intensified and deflected offshore from x=200 m to 400 m. Over 60% bathers with above-average swimming ability can reach the safe depth by swimming against the flow. All the bathers that swim eastward are quickly carried away by the deflected current, and the result is not shown in Fig. 12. Taking the strategy of *swim parallel to shore* alone can not increase the rate of survival in the study. The odds are even heavily against the bathers who choose a wrong direction.

5 Discussions

5.1 Escape strategy summary

The nearshore circulation along the 2 km-long Dadonghai Beach consists of steady longshore currents originated from both headlands, and multiple rip cells pulsating in strength at different time scales. Both types of flows can be hazardous. For swimmers within the inner surf zone, either *swim onshore* or *swim parallel to the beach* can be a wise strategy to escape from the rip flow, while *stay afloat* action may carry the swimmer further away the inner surf zone. Generally a typical rip current ranges from 10-30 m wide. Even a beginning swimmer can reach the neighboring sandbars within 2 min (Figs. 11-12). However, for swimmers located in the outer surf zone, the chance of survival decreases substantially by taking *swim parallel* actions alone. Although many rip hazard outreach activities advocate *swim parallel to the beach* as the primary escape strategy, *swim onshore* seems the most successful strategy across all the scenarios in this study. An average swimmer is capable to reach the safe depth even from the outer surf zone by sustained strokes (Figs. 10). It should be note that the rip strength is

moderate (0.2 - 0.4 m/s on average) for the specified wave conditions in Area 1. Otherwise, the modeling results of Castelle

355   et al. (2016a) indicate that failures of the *swim onshore* occur in the rip neck where swimmers are stuck in the channel due to strong offshore-directed jet.

Stay afloat action can be a viable and energy-saving strategy if the swimmers are within the surf zone with lower exit rate. In this case, most of the swimmers can drift with the circulation cells and remain nearshore. MacMahan et al. (2010) reported that only 19% of the wave drifters deployed in the rip currents exited the surf zone per hour. A 2-day observations conducted

360   by Gallop et al. (2018) found that the exit rates, however, is highly variable from 6% to 71%, depending on the incoming wave breaking and pulsation of surf-zone currents. The results of this study indicate that the surf-zone exit rate is significant higher in this embayed beach, and adopting *stay afloat* action alone is not a wise strategy, with a high risk of being expelled to deeper water (Castelle and Coco, 2013).

Besides, pulsation of rip currents in wide rip channels can form swirls or eddies which can also be hazardous to beginning

365   swimmers or children, especially for those swimming eastwards against the CCE in Area 1. Failure rates of 60% and 78% are observed for beginning swimmers ($U_s = 0.2$ m/s) and children. This suggests that space between sandbars are also an important factor to be considered. In longshore current-dominated nearshore area, *swim onshore* strategy is undoubtedly the optimal action. The mean duration to safety is only 1.2 min for an average swimmer.

5.2   Lagrangian tracking by wave-resolving and mean-flow velocities

370   In FUNWAVE-TVD, the random directional wave field is generated by using an internal wavemaker. It is basically an interior source term which integrates wave components split by frequency, direction and with random phases (Wei et al., 1999). The input for the wavemaker can be either wave bulk parameters (i.e., peak wave height and period), or TMA shallow-water spectrum. In the study, swimmers are tracked by instantaneous velocity at the time interval $\triangle t$ of 0.04 s, rather than the wave-averaged velocity (i.e., averaging phase-resolving velocity over 24 s). It results in jagged trajectories shown in Fig. 9-12. Due

375   to the random nature of wave field, the trajectory of each seeded swimmer is composed of a slow meander that exhibits mean flow pattern, and a much faster random oscillation at a wave time scale. One remaining question is whether wave-resolving and mean-flow tracing of individual swimmer can reproduce consistent trajectories, and whether the difference between the trajectories can be ignored so that it do not affect the conclusion of escaping modeling in the study. In Fig. 13, a 10-min tracking of virtual swimmers by instantaneous and wave-averaged velocity is illustrated with two overlapped curves (light and

380   dark gray lines). The ends of each pair of trajectories are connected by orange lines. Fig. 13a-b suggest that resolving wave scale in the Lagrangian tracking produces comparable statistical results of escape time (t_{safe}) with that using the mean-flow velocity in general (Fig. 13c-d). Nevertheless, effect of wave randomness on individual trajectories can be observed, which results in different floating paths for a few virtual swimmers (denoted by long orange line segments).

5.3   Sensitivity analysis on the wave-following factor c_f

385   In Equation 1, a coefficient controlling how well a swimmer drifts with the ambient wave-induced flows is defined as the wave-following factor c_f. A value of 0.8 is assigned following the previous studies (McCarroll et al., 2015; Castelle et al.,

2016a). However, this value has not been well calibrated by field researches. A sensitivity study of the factor is carried out in this modeling study by vary its value from 0.4 to 1.0 with an interval of 0.2. Among these values, c_f=1.0 denotes that swimmers float with the flow perfectly when swimming actively, while c_f=0.4 means they are less influenced by the ambient flows. Swimmer tracking simulations with varying c_f values for strategy of *swimming onshore* within Area 1 are conducted and the modeling results are summarized in Fig. 14. A constant onshore swimming velocity of 0.2 m/s is adopted.

In Fig. 14, the prominent feature is that the amount of swimmers who fail to reach safety decreases as the floating factor is assigned with smaller values (trajectories and bars with red color in the figure). In the case of c_f=0.4, almost entire seeded swimmers can escape from the rip eddy and swim to safe areas in less than 10 min, even for those seeded at rip neck and downdrift of rip eddy. However, the failure rate can reach over 40% if the floating factor of 1.0 is set in the tracking module. The results of this sensitivity analysis highlight the uncertainties of the tracking simulations. It is essential to calibrate this coefficient in the further field studies.

6 Conclusions

This paper presents the results of a Boussinesq modeling of rip hazard and escape strategies in an embayed recreational beach with grid resolution of 1 m. Especially, discussions have been made on the variability of rip currents, how wave-resolving tracking of virtual swimmers differs from that using mean flow velocity, as well as sensitivity of tracking results on the wave-following factor c_f.

Beach stage plays an important role in the occurrence and strength of rip currents (Dalrymple et al., 2011). Surf-zone bathymetry obtained in 2018 and 2019 exhibits different beach stages. The modeling results show that shore-connected trans-verse bars with incised, narrow rip channels are favorable to strong rip cells, while the crescentic bars separated by rip troughs with shallow exits, though, generate more complex yet slightly weaker nearshore circulations. A series of Boussinesq mod-elings indicate that rip current strength is closely related to several incoming wave properties, including wave height, peak period, and incident angles. Tidal level also exhibits the modulating effect on rip strength. The results agree with the previous studies on variability of rip currents. Spectral analysis of the output time series shows that rip currents fluctuate on the orders of 1 min and 10 min, which reflects the effects of wave-group and VLF motions. The pulsation of rip currents has importance for beach safety.

Quantitative estimate rip hazard has been enabled by the high-resolution modeling of nearshore circulation. In this study we defined a four-level rip hazard indexes based on a combination of rip flow strength and its duration. With the state-of-art GPU computation facility, operational forecasting of rip hazard level now is possible within 20 min based on the FUNWAVE-GPU embedded to GPU-accelerated spectral wave model on an commercially-available PC.

Outcomes of the modeling demonstrate that multiple factors contributing to the survival of swimmers being caught in the rip currents, include surf-zone bathymetry, rip strength, flow patterns, bather's position and swimming ability. Considering the temporal and spatial variability of nearshore circulation, neither strategy is 100% successful, and a combination of different actions is necessary for specific occasions. For weak-to-moderate rip currents and longshore currents, *swim onshore* consis-

tently seems the most successful strategy across all the scenarios in this study. For swimmers within the inner surf zone, the successful rate is satisfactory by taking strategies of either *swim onshore* or *swim parallel to the beach*. To reduce risk at the shoreline, simply educating the public to stay inside the inner surf zone and enter water with buoyancy is a basic rule. *Stay afloat* action can be a viable and energy-saving strategy if the swimmers are within the surf zone with lower exit rate. However, floating generally resulted in longer times to safety with higher variability compared to swimming parallel or onshore. The surf-zone exit rates are high variable depending on individual beach stages and incoming wave conditions. Our results indicate that adopting *stay afloat* action alone may lower the chance of escape, and suffer a high risk of being expelled to deeper water. Besides, pulsation of rip currents in wide rip channels can form swirls or eddies which can also be hazardous to swimmers with weak swimming ability. This suggests that space between sandbars are also an important factor to be considered. Psychological factors also contribute to the rip escape, which is not discussed in the study.

There are two primary types of models that are used to simulate surf zone flows. While the majority of the rip-current studies used short-wave-averaged model, in this study we used the Boussinesq model which required higher grid resolution to resolve wave crests. Wave-resolving Lagrangian tracking helps us understand the effect of wave randomness on surf-zone flows and bathers' trajectories. It should be noted that lack of field observations largely limits our analysis of fine-scale rip current dynamics at the Dadonghai Beach. Besides, sensitivity study on assignment of wave-following coefficient of virtual swimmers c_f showcases large uncertainties of the Lagrangian tracking simulations in the study, which also urges a comprehensive field campaign on rip currents and associated hazards in the future at this rip-prone area.

Author contributions. The manuscript was written by Ye Yuan. FUNWAVE-TVD was GPU-accelerated by Ye Yuan when visiting University of Delaware in 2019. The computation and visualization were carried out by Huaiwei Yang. Fujiang Yu conceived the research. Surf-zone bathymetry was mapped by Yi Gao using Satellite images obtained from Google Earth. Benxia Li and Chuang Xing processed the wave analysis data.

Competing interests. The authors declare that they have no conflict of interest.

Acknowledgements. The work is supported by the Innovative Youth Talents Program, MNR of China, as well as National Science and Technology Major Project of China (Grant no. 2016YFC14015).

References

445   Arun Kumar, S. V. V. and Prasad, K. V. S. R.: Rip current-related fatalities in India: a new predictive risk scale for forecasting rip currents, Natural Hazards, 70, 313–335, https://doi.org/10.1007/s11069-013-0812-x, 2014.

Bowen, A. J.: Rip currents: 1. Theoretical investigations, Journal of Geophysical Research (1896-1977), 74, 5467–5478, https://doi.org/10.1029/JC074i023p05467, 1969.

Brewster, B. C., Gould, R. E., and Brander, R. W.: Estimations of rip current rescues and drowning in the United States, Natural Hazards and
450   Earth System Sciences, 19, 389–397, https://doi.org/10.5194/nhess-19-389-2019, 2019.

Brighton, B., Sherker, S., Brander, R., Thompson, M., and Bradstreet, A.: Rip current related drowning deaths and rescues in Australia 2004–2011, Natural Hazards and Earth System Sciences, 13, 1069–1075, https://doi.org/10.5194/nhess-13-1069-2013, 2013.

Castelle, B. and Coco, G.: Surf zone flushing on embayed beaches, Geophysical Research Letters, 40, 2206–2210, https://doi.org/10.1002/grl.50485, 2013.

455   Castelle, B., McCarroll, R., Brander, R., T., S., and B., D.: Modelling the alongshore variability of optimum rip current escape strategies on a multiple rip-channelled beach, Nat Hazards, 81, 663–686, https://doi.org/10.1007/s11069-015-2101-3, 2016a.

Castelle, B., Scott, T., Brander, R., and McCarroll, R.: Rip current types, circulation and hazard, Earth-Science Reviews, 163, 1–21, https://doi.org/10.1016/j.earscirev.2016.09.008, 2016b.

Castelle, B., Scott, T., Brander, R., McCarroll, R. J., Tellier, E., de Korte, E., Tackuy, L., Robinet, A., Simonnet, B., and Salmi, L.-R.: Wave
460   and Tide Controls on Rip Current Activity and Drowning Incidents in Southwest France, Journal of Coastal Research, 95, 769 – 774, https://doi.org/10.2112/SI95-150.1, 2020.

Chen, Q., Dalrymple, R. A., Kirby, J. T., Kennedy, A. B., and Haller, M. C.: Boussinesq modeling of a rip current system, Journal of Geophysical Research: Oceans, 104, 20 617–20 637, https://doi.org/10.1029/1999jc900154, 1999.

Chen, Q., Kirby, J. T., Dalrymple, R. A., Shi, F., and Thornton, E. B.: Boussinesq modeling of longshore currents, Journal of Geophysical
465   Research: Oceans, 108, 3362, https://doi.org/10.1029/2002JC001308, 2003.

Dalrymple, R. A., MacMahan, J. H., Reniers, A. J., and Nelko, V.: Rip Currents, Annual Review of Fluid Mechanics, 43, 551–581, https://doi.org/10.1146/annurev-fluid-122109-160733, 2011.

Dusek, G. and Seim, H.: A Probabilistic Rip Current Forecast Model, Journal of Coastal Research, 29, 909–925, https://doi.org/10.2307/23486560, 2013.

470   Engle, J. A., MacMahan, J. H., Thieke, R. J., Hanes, D. M., and Dean, R. G.: Formulation of a Rip Current Predictive Index Using Rescue Data, in: Tsunamis: Geology, Hazards and Risks, 2002.

Eom, H., Yun, J. H., Jeong, C. K., Seo, J. W., and You, S. H.: Introduction to KMA Operational Forecasting System for Rip Current, Journal of Coastal Research, pp. 63–68, https://doi.org/10.2112/SI72-012.1, 2014.

Feddersen, F.: The Generation of Surfzone Eddies in a Strong Alongshore Current, Journal of Physical Oceanography, 44, 600 – 617,
475   https://doi.org/10.1175/JPO-D-13-051.1, 2014.

Gallop, S., Bryan, K., Pitman, S., Ranasinghe, R., and Harrison, S.: Rip current circulation and surf zone retention on a double barred beach, Marine Geology, 405, 12–22, https://doi.org/10.1016/j.margeo.2018.07.015, 2018.

Geiman, J. D., Kirby, J. T., Reniers, A. J. H. M., and MacMahan, J. H.: Effects of wave averaging on estimates of fluid mixing in the surf zone, Journal of Geophysical Research: Oceans, 116, C04 006, https://doi.org/10.1029/2010JC006678, 2011.

480   Group, T. W.: The WAM Model—A Third Generation Ocean Wave Prediction Model, Journal of Physical Oceanography, 18, 1775 – 1810, https://doi.org/10.1175/1520-0485(1988)018, 1988.

Kennedy, A. B., Chen, Q., Kirby, J. T., and Dalrymple, R. A.: Boussinesq Modeling of Wave Transformation, Breaking, and Runup. I: 1D, Journal of Waterway, Port, Coastal, and Ocean Engineering, 126, 39–47, https://doi.org/10.1061/(ASCE)0733-950X(2000)126:1(39), 2000.

485   Kim, I., Lee, J., and Lee, J.: Verification of Rip Current Simulation Using a Two-Dimensional Predictive Model, HAECUM, Journal of Coastal Research, 65(sp1), 726–730, https://doi.org/10.2112/SI65-123.1, 2013.

Kirby, J. T.: Boussinesq models and their application to coastal processes across a wide range of scales, Journal of Waterway, Port, Coastal, and Ocean Engineering, 142, 03116 005, https://doi.org/10.1061/(ASCE)WW.1943-5460.0000350, 2016.

Li, Z.: Rip current hazards in South China headland beaches, Ocean and Coastal Management, 121, 23–32,
490   https://doi.org/10.1016/j.ocecoaman.2015.12.005, 2016.

Li, Z. and Zhu, S.: Why There Are So Many Drowning Accidents Happened at Dadonghai Beach, Hainan, China: Morphodynamic Analysis, Journal of Coastal Research, 85, 741–745, https://doi.org/10.2112/SI85-149.1, 2018.

MacMahan, J., Brown, J., Brown, J., Thornton, E., Reniers, A., Stanton, T., Henriquez, M., Gallagher, E., Morrison, J., Austin, M. J., Scott, T. M., and Senechal, N.: Mean Lagrangian flow behavior on an open coast rip-channeled beach: A new perspective, Marine Geology, 268,
495   1–15, https://doi.org/10.1016/j.margeo.2009.09.011, 2010.

MacMahan, J. H., Reniers, A. J. H. M., Thornton, E. B., and Stanton, T. P.: Infragravity rip current pulsations, Journal of Geophysical Research: Oceans, 109, C01 033, https://doi.org/10.1029/2003JC002068, 2004a.

MacMahan, J. H., Reniers, A. J. H. M., Thornton, E. B., and Stanton, T. P.: Surf zone eddies coupled with rip current morphology, Journal of Geophysical Research: Oceans, 109, C07 004, https://doi.org/10.1029/2003JC002083, 2004b.

500   MacMahan, J. H., Thornton, E. B., and Reniers, A. J.: Rip current review, Coastal Engineering, 53, 191–208, https://doi.org/10.1016/j.coastaleng.2005.10.009, 2006.

Masselink, G. and Short, A. D.: The effect of tide range on beach morphodynamics and morphology: a conceptual beach model, Journal of Coastal Research, 9, 785–800, 1993.

McCarroll, R. J., Brander, R. W., MacMahan, J. H., Turner, I. L., Reniers, A. J., Brown, J. A., Bradstreet, A., and Sherker, S.: Evaluation of
505   swimmer-based rip current escape strategies, Natural Hazards, 71, 1821–1846, https://doi.org/10.1007/s11069-013-0979-1, 2014.

McCarroll, R. J., Castelle, B., Brander, R., and T., S.: Modelling rip current flow and bather escape strategies across a transverse bar and rip channel morphology, Geomorphology, 246, 502–518, https://doi.org/10.1016/j.geomorph.2015.06.041, 2015.

Radermacher, M., de Schipper, M., and Reniers, A.: Sensitivity of rip current forecasts to errors in remotely-sensed bathymetry, Coastal Engineering, 135, 66–76, https://doi.org/10.1016/j.coastaleng.2018.01.007, 2018.

510   Reniers, A. J. H. M., MacMahan, J. H., Beron-Vera, F. J., and Olascoaga, M. J.: Rip-current pulses tied to Lagrangian coherent structures, Geophysical Research Letters, 37, L05 605, https://doi.org/10.1029/2009GL041443, 2010.

Shepard, F. P.: Undertow, Rip Tide or "Rip Current", Science, 84, 181–182, https://doi.org/10.1126/science.84.2173.181, 1936.

Shi, F., Kirby, J. T., Harris, J. C., Geiman, J. D., and Grilli, S. T.: A high-order adaptive time-stepping TVD solver for Boussinesq modeling of breaking waves and coastal inundation, Ocean Modelling, 43-44, 36–51, https://doi.org/10.1016/j.ocemod.2011.12.004, 2012.

515   Tian, D., Zhang, H., Zhang, W., Zhou, F., Sun, X., Zhou, Y., and Ke, D.: Wave Glider Observations of Surface Waves During Three Tropical Cyclones in the South China Sea, Water, 12, 1331, https://doi.org/10.3390/w12051331, 2020.

Tonelli, M. and Petti, M.: Hybrid finite volume - finite difference scheme for 2DH improved Boussinesq equations, Coastal Engineering, 56, 609–620, https://doi.org/10.1016/j.coastaleng.2009.01.001, 2009.

Van Leeuwen, B. R., McCarroll, R. J., Brander, R. W., Turner, I. L., Power, H. E., and Bradstreet, A. J.: Examining rip current escape
520   strategies in non-traditional beach morphologies, Natural Hazards, 81, 145–165, https://doi.org/10.1007/s11069-015-2072-4, 2016.

Wang, H., Zhu, S., Li, X., Zhang, W., and Nie, Y.: Numerical simulations of rip currents off arc-shaped coastlines, Acta Oceanologica Sinica, 37, 21–30, https://doi.org/10.1007/s13131-018-1197-1, 2018.

Wei, G., Kirby, J. T., and Sinha, A.: Generation of waves in Boussinesq models using a source function method, Coastal Engineering, 36, 271–299, https://doi.org/10.1016/S0378-3839(99)00009-5, 1999.

525 Wright, L. and Short, A.: Morphodynamic variability of surf zones and beaches: A synthesis, Marine Geology, 56, 93–118, https://doi.org/10.1016/0025-3227(84)90008-2, 1984.

Xu, Y., He, H., Song, J., Hou, Y., and Li, F.: Observations and Modeling of Typhoon Waves in the South China Sea, Journal of Physical Oceanography, 47, 1307 – 1324, https://doi.org/https://doi.org/10.1175/JPO-D-16-0174.1, 2017.

Yuan, Y., Shi, F., Kirby, J. T., and Yu, F.: FUNWAVE-GPU: Multiple-GPU Acceleration of a Boussinesq-Type Wave Model, Journal of
530   Advances in Modeling Earth Systems, 12, e2019MS001 957, https://doi.org/10.1029/2019MS001957, 2020.

Zhang, Y., Huang, W., Liu, X., Zhang, C., Xu, G., and Wang, B.: Rip current hazard at coastal recreational beaches in China, Ocean and Coastal Management, 210, 105 734, https://doi.org/10.1016/j.ocecoaman.2021.105734, 2021.

Zhang, Y., Shi, F., Kirby, J. T., and Feng, X.: Phase-Resolved Modeling of Wave Interference and Its Effects on Nearshore Circulation in a Large Ebb Shoal-Beach System, Journal of Geophysical Research: Oceans, 127, e2022JC018 623, https://doi.org/10.1029/2022JC018623,
535   2022.
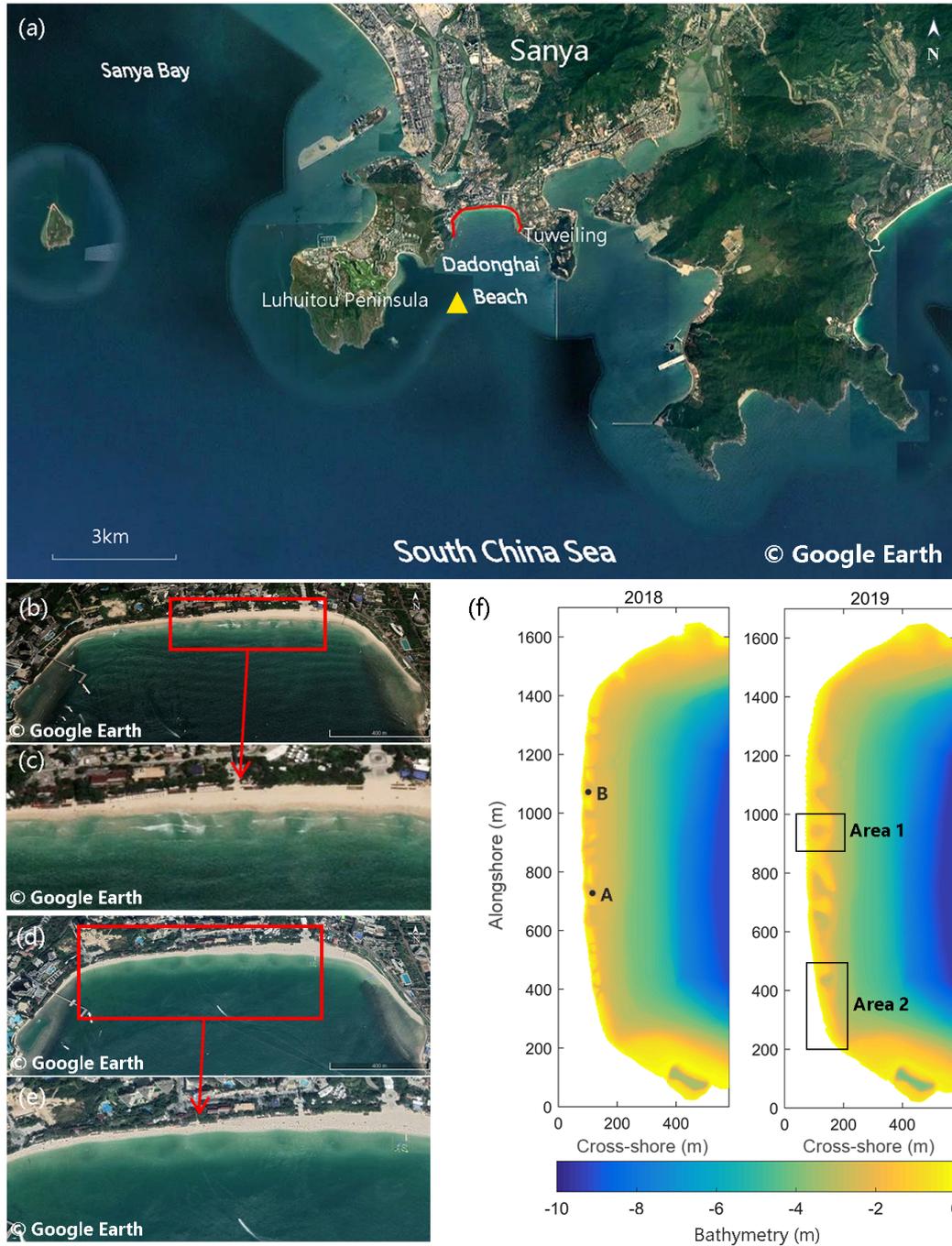
Figure 1. Location map of the Dadonghai Beach, Sanya (a), with satellite images collected on August 7, 2018 and December 26, 2019 (b-e). The satellite-derived bathymetry contours with spatial resolution of 1 m are displayed with orientation rotated 90 degree clockwise (f). Gauge A and Gauge B are set to investigate rip current variability. Virtual swimmers are evenly seeded within Area 1 and 2 marked by two red rectangles, with the purpose of studying swimmer escape strategies. The wave hindcast point is denoted as yellow triangle. The image source is Google Earth.
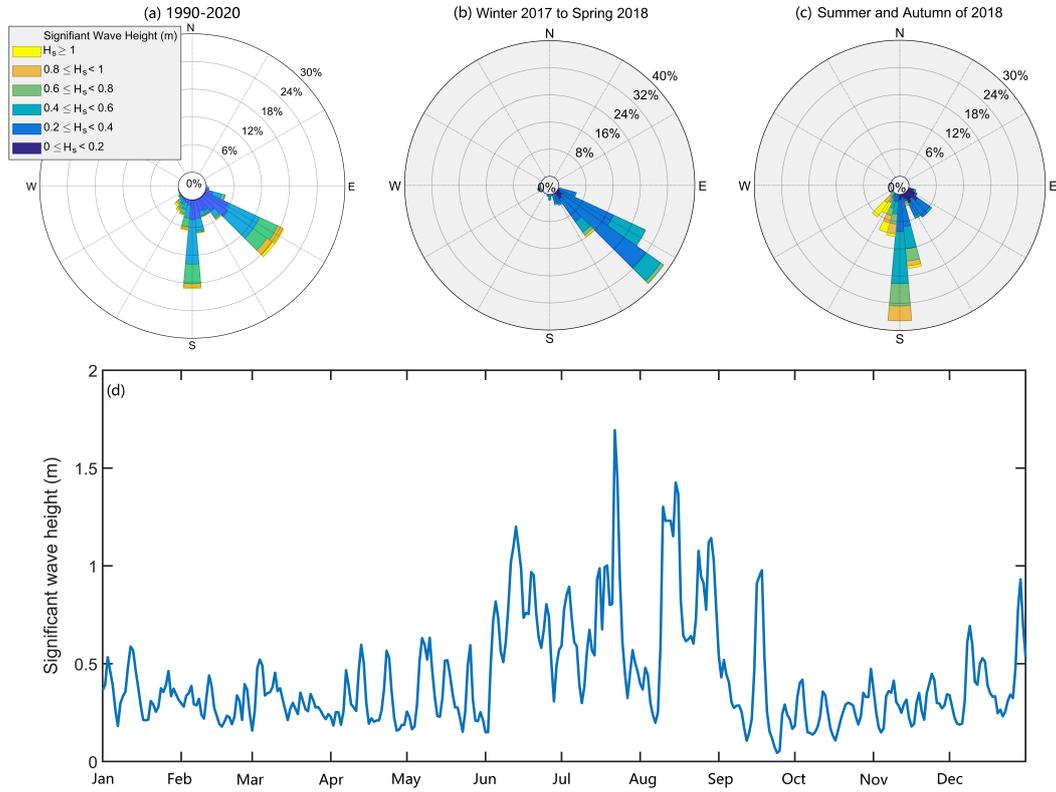
Figure 2. Wave climate in study site. Subplot (a) is wave rose diagram of 30-year-long time series of wave hindcast at a wave point immediately off the Dadonghai Bay (109.5° E, 18.2° N); (b-c) are wave rose diagrams for winter monsoon and summer typhoon seasons, respectively; (d) is 1 day-averaged time series of significant wave height in 2018.
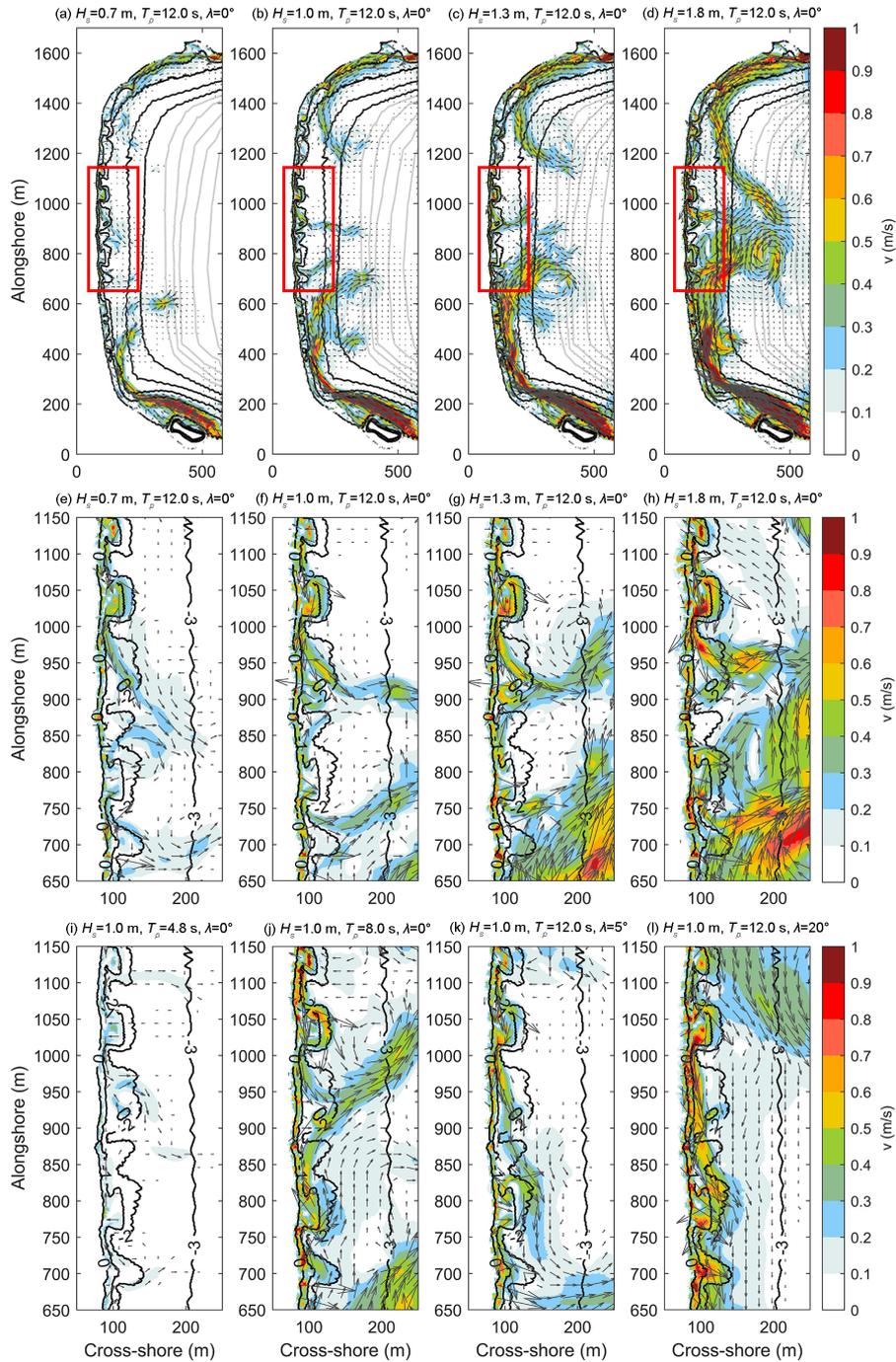
Figure 3. Snapshot of wave-driven velocity field in the embayed Dadonghai Beach with different forcing wave conditions labeled in the top of each subplot. Rip flows within the red rectangle in subplot (a-d) is enlarged in (e-l). Bathymetry is acquired on August 7, 2018 (corresponding to Fig. 1b-c, and characterized by transverse bars incised by relatively deep rip channels. Depth contours are overlapped as thick, black lines.
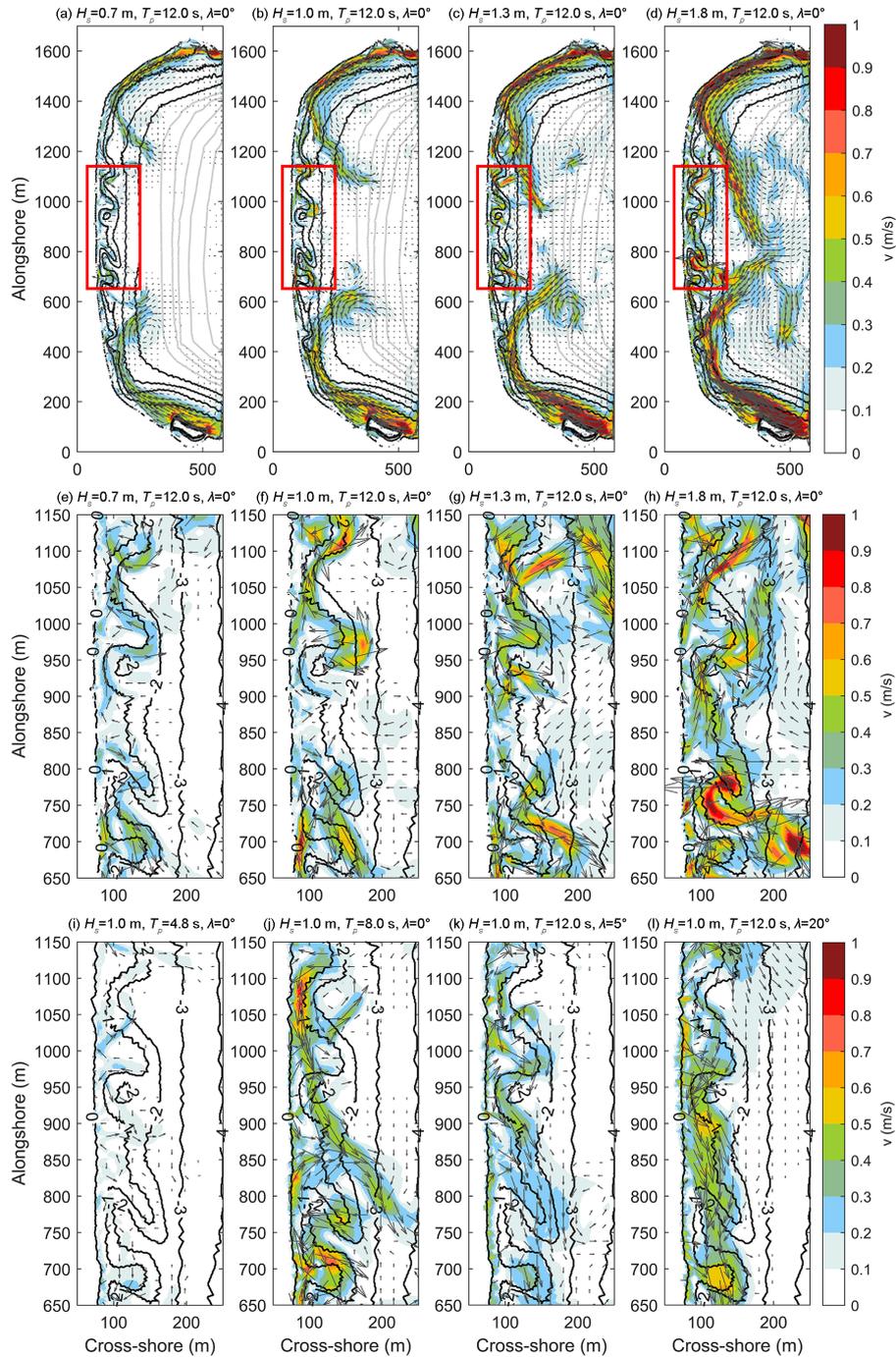
Figure 4. Snapshot of wave-driven velocity field in the embayed Dadonghai Beach with different forcing wave conditions labeled in the top of each subplot. Bathymetry is acquired on December 26, 2019 (corresponding to Figure 1d-e), and characterized by crescentic outer bars with periodic shallow and wide troughs.
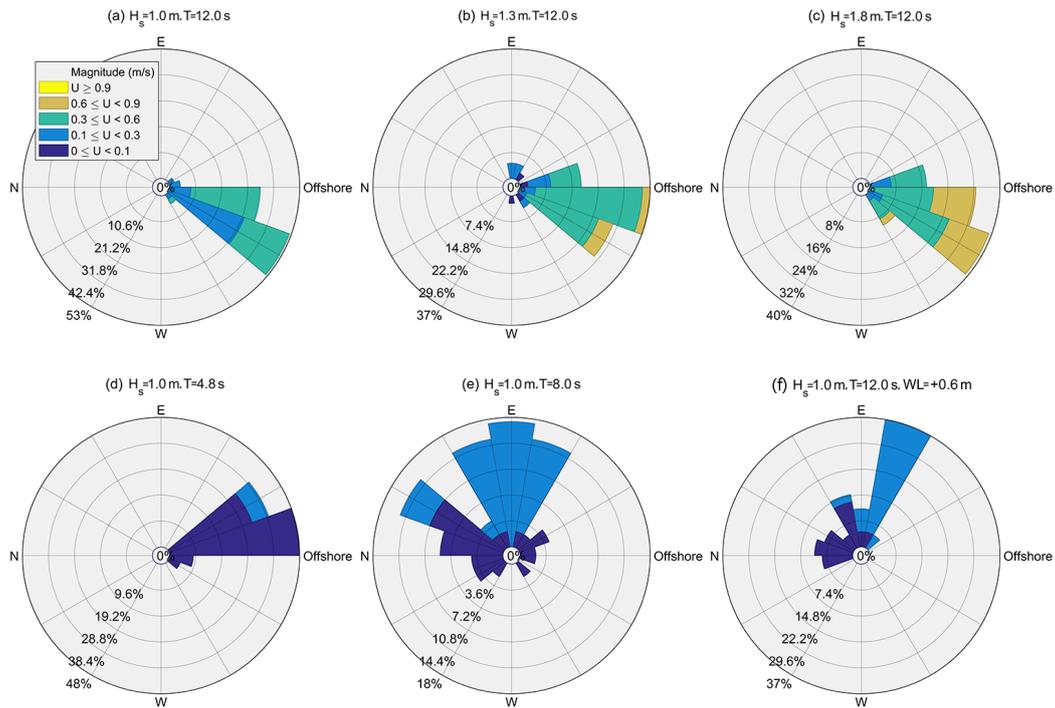
Figure 5. Rip current rose diagrams of rip currents forced by different wave conditions and tidal level at position x = 730 m and y = 120 m marked as Gauge A in Fig. 1f. Each spoke denotes the direction that the current flows to. The offshore direction is labeled in each diagram. T1 and T7-8 are not included.
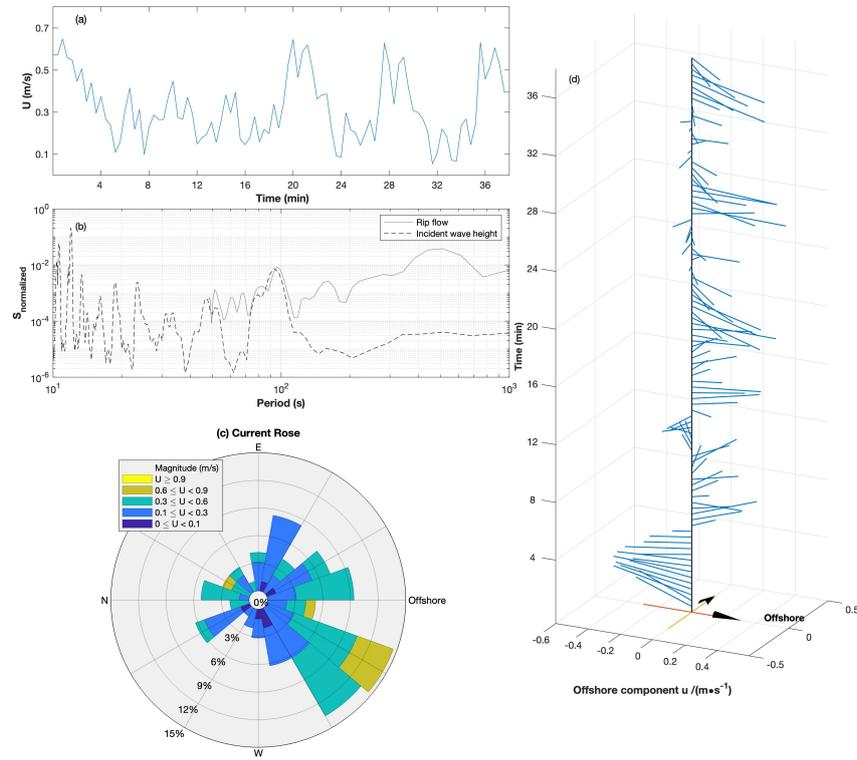
Figure 6. Analysis of rip flow variability in Gauge B: time series starting from 900 s (a); power spectra of rip flow and incident wave height (b); rose diagram and vector plot of Gauge B (c-d). The location of Gauge B is marked in Fig. 1f
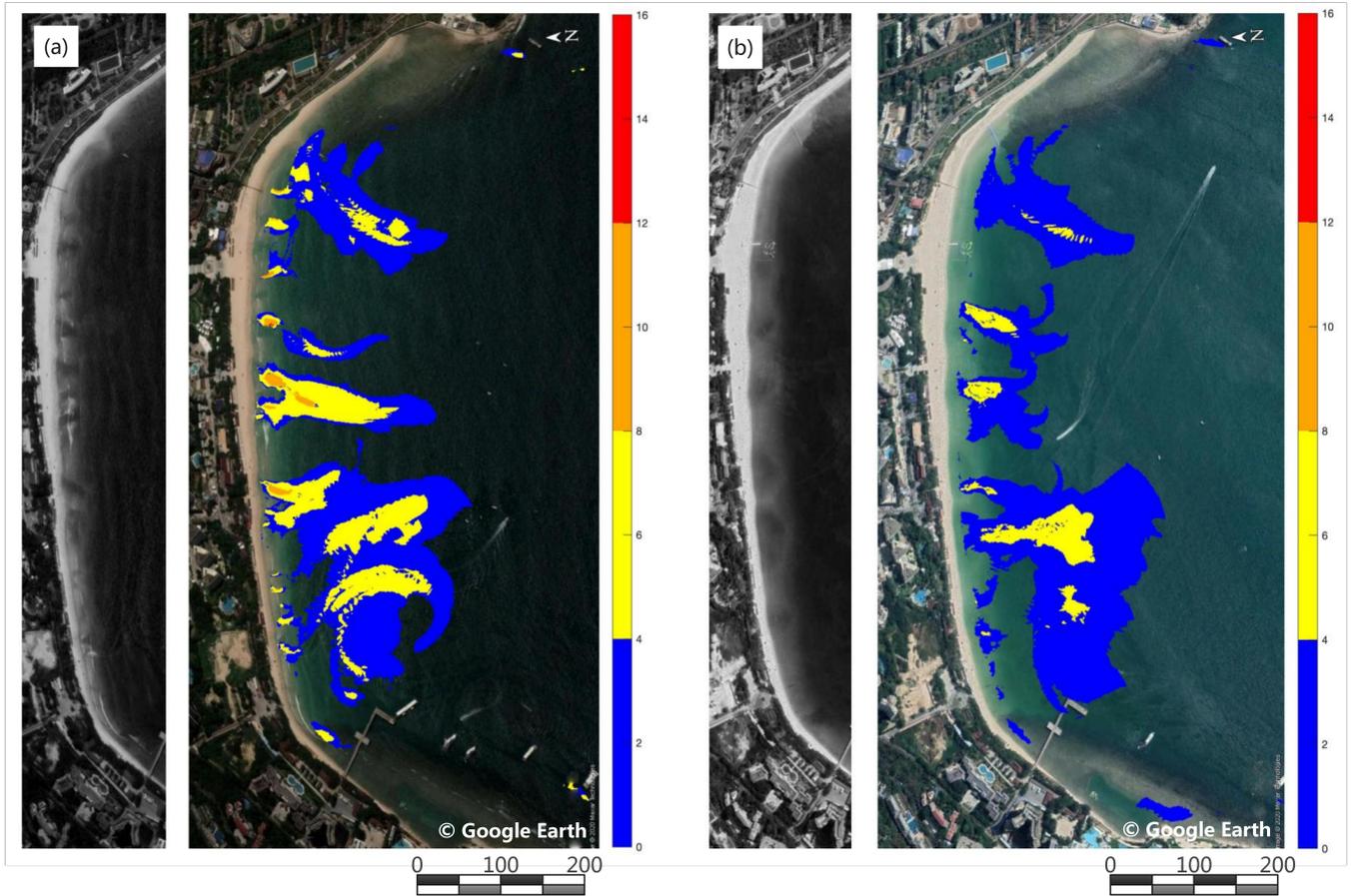
Figure 7. Rip hazard maps for shore-normal incident waves of H_s = 1.0 m, and T_p = 12 s (corresponding to T2 with mean tidal level) at the Dadonghai Beach, using bathymetry on August 7, 2018 (a) and December 26, 2019 (b).
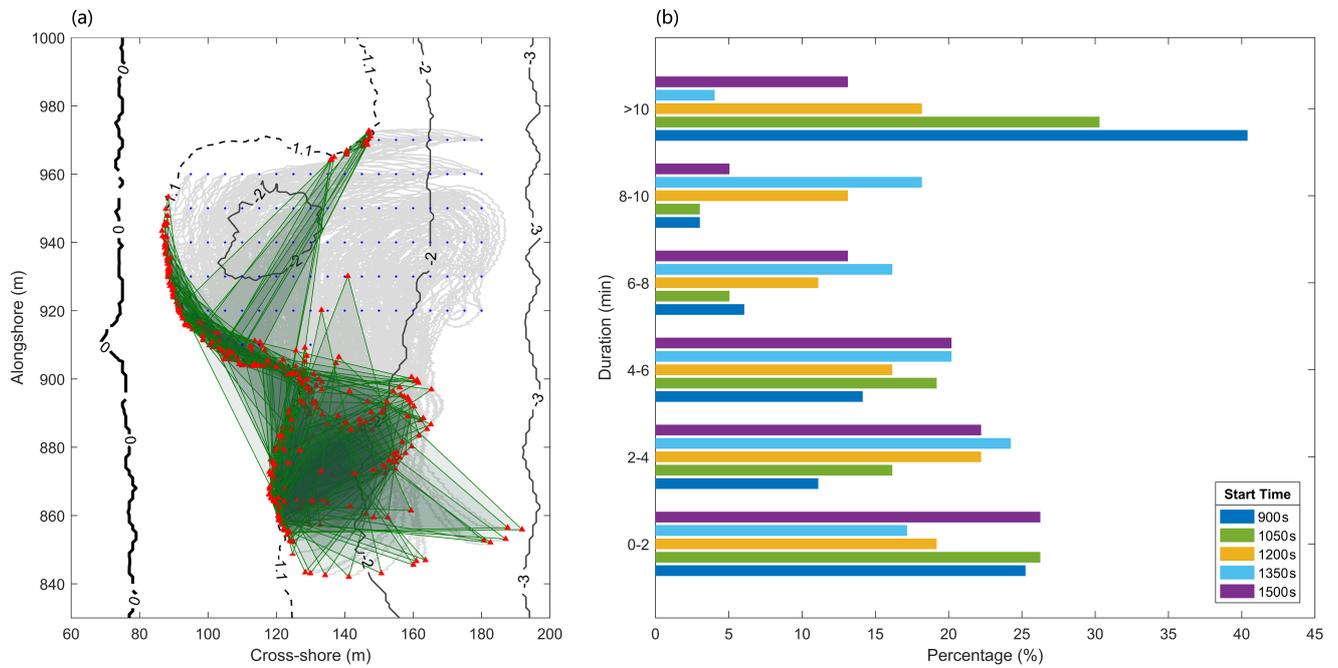
Figure 8. Lagrangian tracking of the virtual swimmers seeded at 5 different modeling times (with an interval of 150 s from 900 s to 1500 s) within Area 1 (a). Histograms of t_{safe} given in percentages of swimmers who have reached safety at each t_{safe} range, is shown in subplot (b). The initial seeding positions are marked by blue dots. At each position, the resulting 5 trajectories are plotted as light gray lines, with their ends (red triangles) connected by green lines. The shaded polygons are to highlight the variability of tracking outcomes. Surf-zone bathymetry is contoured as black lines.

Stay afloat
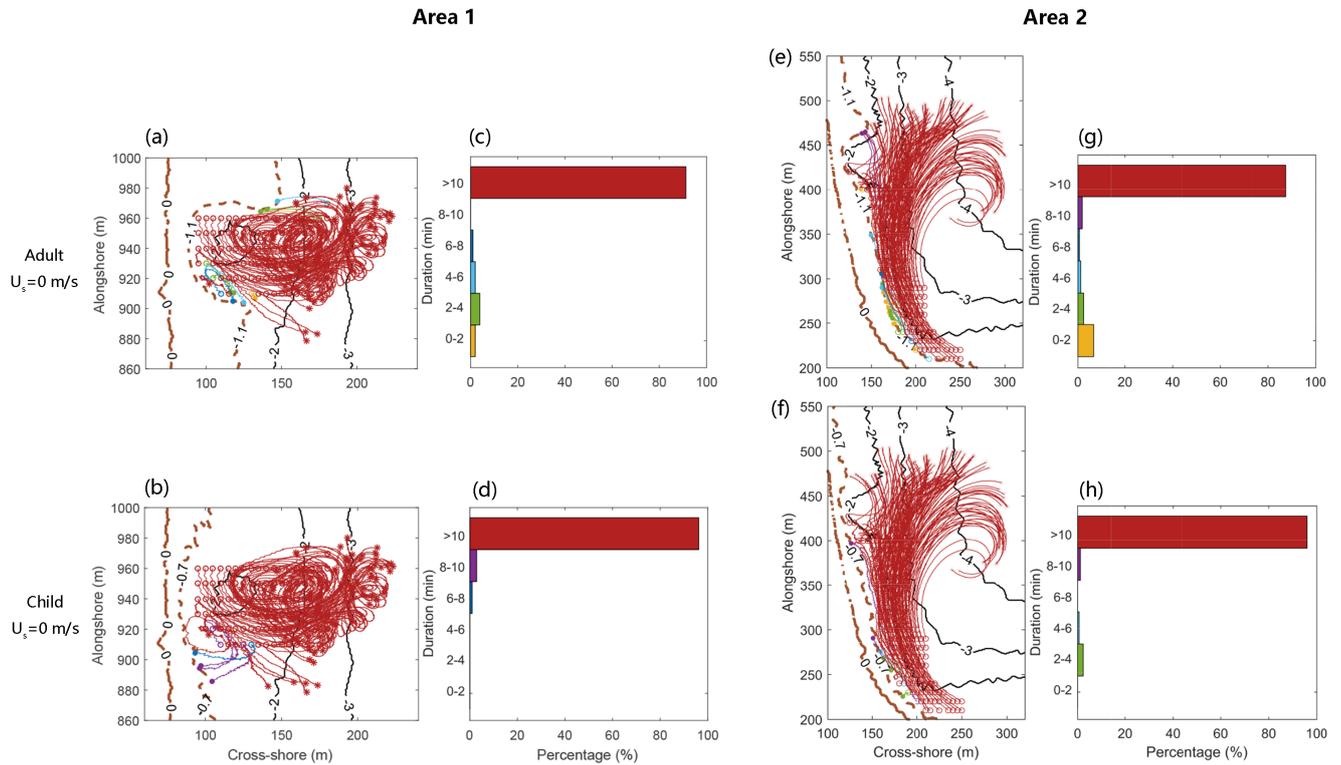
Figure 9. Swimmer tracking simulations for strategy of *stay afloat* within Area 1 (left panel), and Area 2 (right panel). Histograms of t_{safe} give percentages of swimmers who have reached safety at each t_{safe} range. The trajectories of swimmers have colors corresponding to bins in each histogram. Surf-zone bathymetry is contoured as black solid lines and brown dashed lines (0, 0.7 and 1.1 coutour lines).

Swim onshore
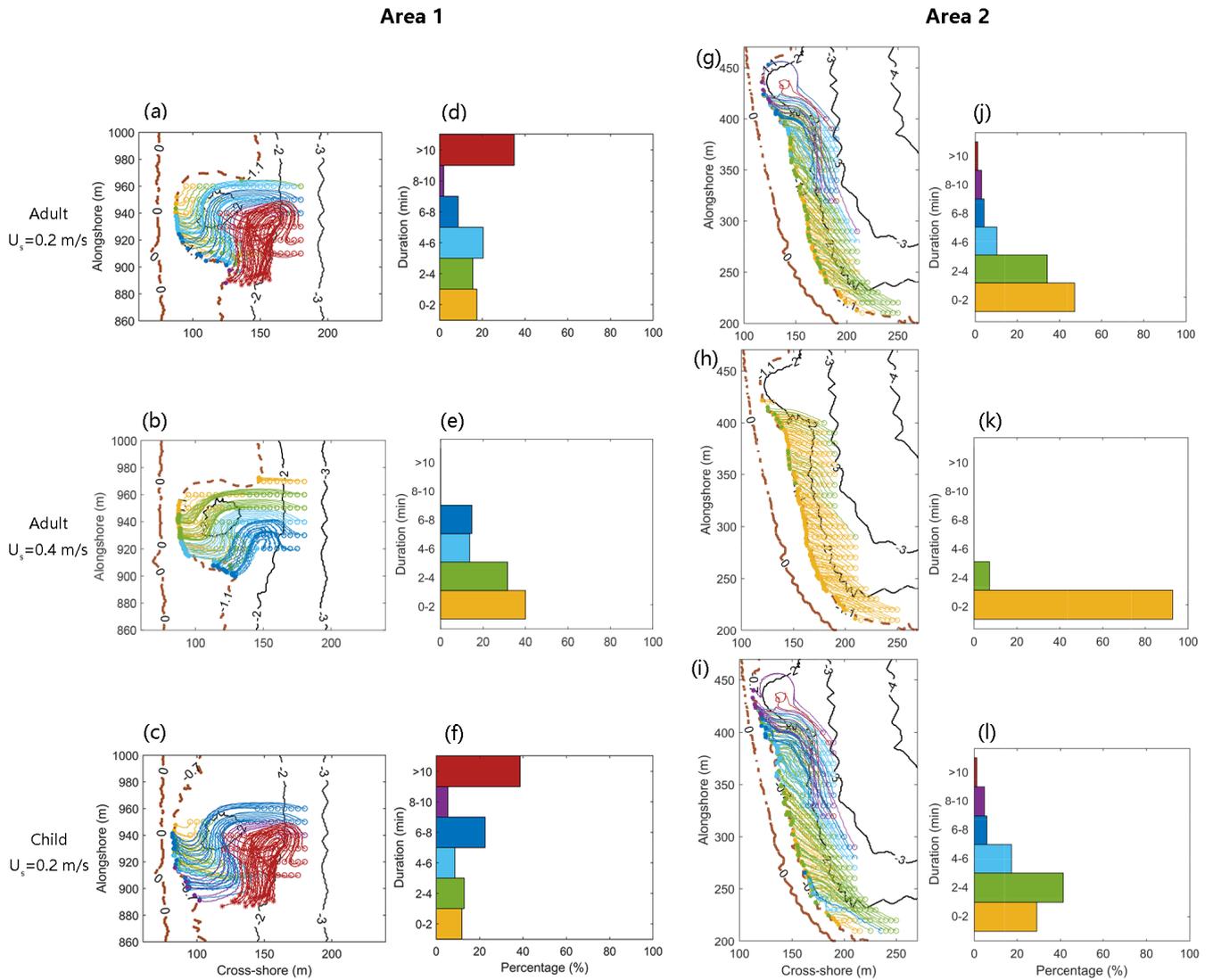
Figure 10. Swimmer tracking simulations for strategy of *swimming Onshore* within Area 1 (left panel), and Area 2 (right panel). Histograms of t_{safe} give percentages of swimmers who have reached safety at each t_{safe} range. The trajectories of swimmers have colors corresponding to bins in each histogram. Surf-zone bathymetry is contoured as black solid lines and brown dashed lines (0, 0.7 and 1.1 coutour lines).

Swim parallel
(Westward)

Area 1   Area 2
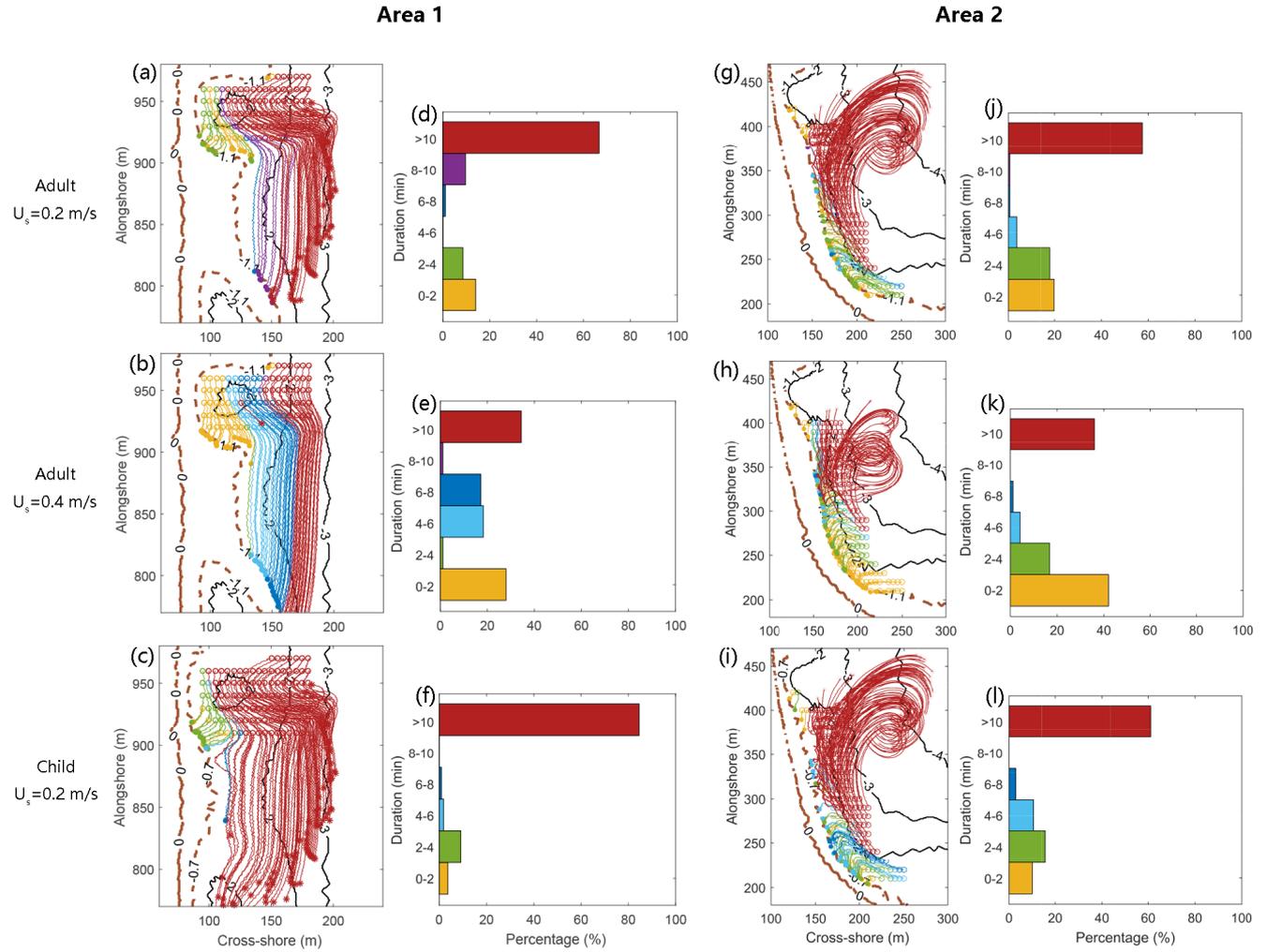
Figure 11. Swimmer tracking simulations for strategy of *swimming westward parallel to shore* within Area 1 (left panel), and Area 2 (right panel). Histograms of t_{safe} give percentages of swimmers who have reached safety at each t_{safe} range. The trajectories of swimmers have colors corresponding to bins in each histogram. Surf-zone bathymetry is contoured as black solid lines and brown dashed lines (0, 0.7 and 1.1 coutour lines).

Swim parallel (Eastward)
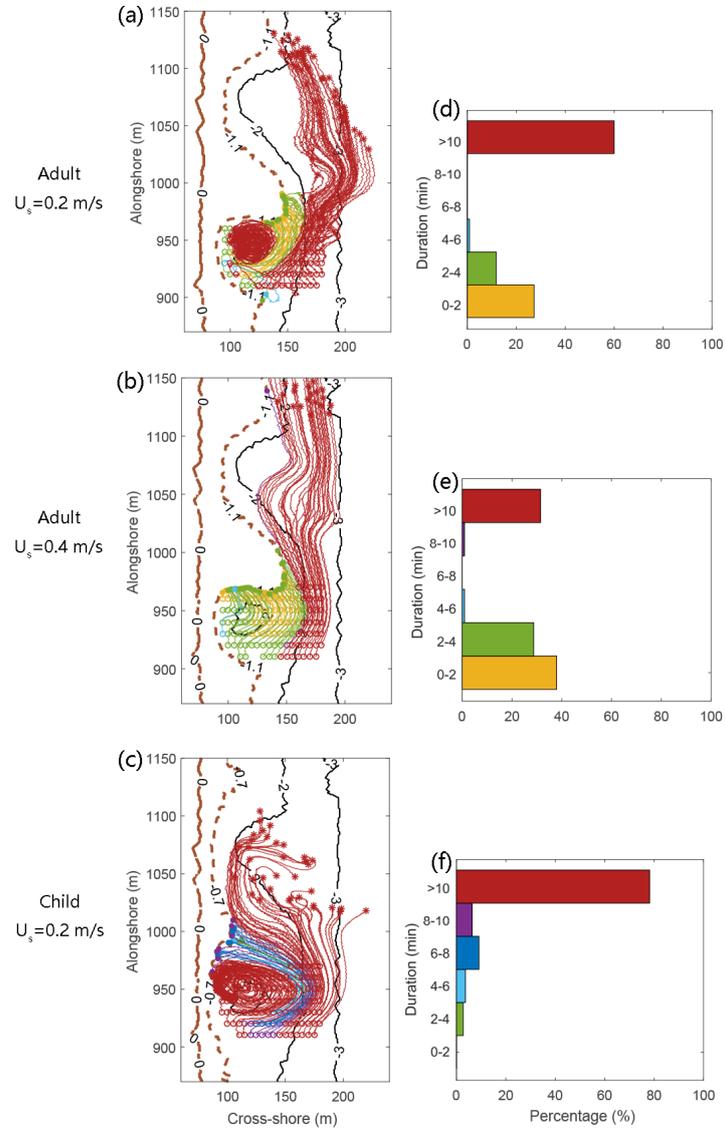
Area 1

Figure 12. Swimmer tracking simulations for strategy of *swimming eastward parallel to shore* within Area 1. Histograms of t_{safe} give percentages of swimmers who have reached safety at each t_{safe} range. The trajectories of swimmers have colors corresponding to bins in each histogram. Surf-zone bathymetry is contoured as black solid lines and brown dashed lines (0, 0.7 and 1.1 coutour lines).
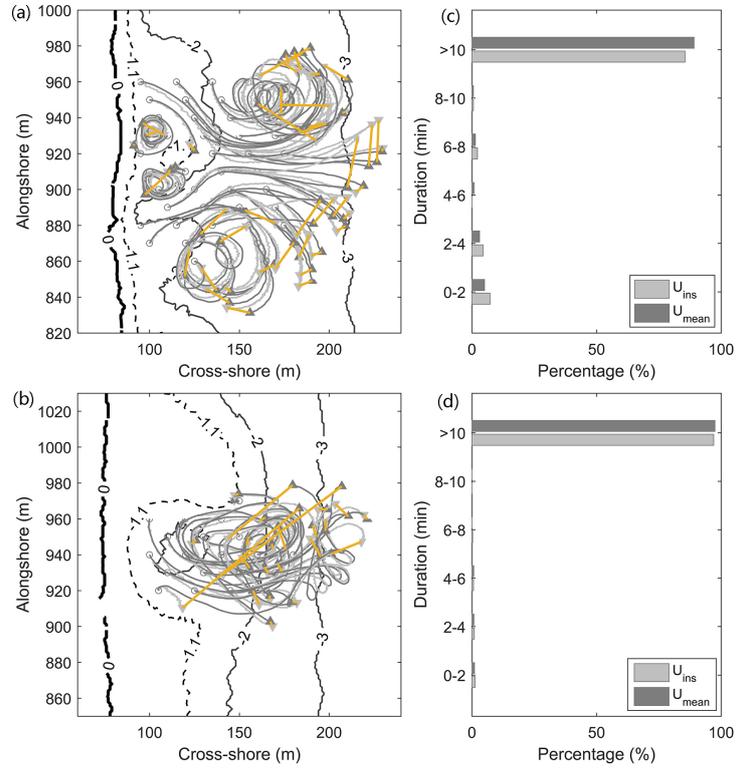
Figure 13. 10-min swimmer tracking simulations by instantaneous velocity (light gray line with start and end marked by open circles and solid triangles) and 24 s-averaged mean velocity (dark gray line), respectively. The ends of each pair of trajectories are connected by orange lines to denote the difference of tracking. Surf-zone bathymetry obtained in 2018 (top panel) and 2019 (lower panel) in Area 1 are used, which is overlapped by black contour lines. Histograms of t_{safe} (right subplots) give percentages of swimmers who have reached safety at each t_{safe} range. U_{ins} and U_{mean} denote the instantaneous and wave-averaged velocity, respectively.

Swim onshore
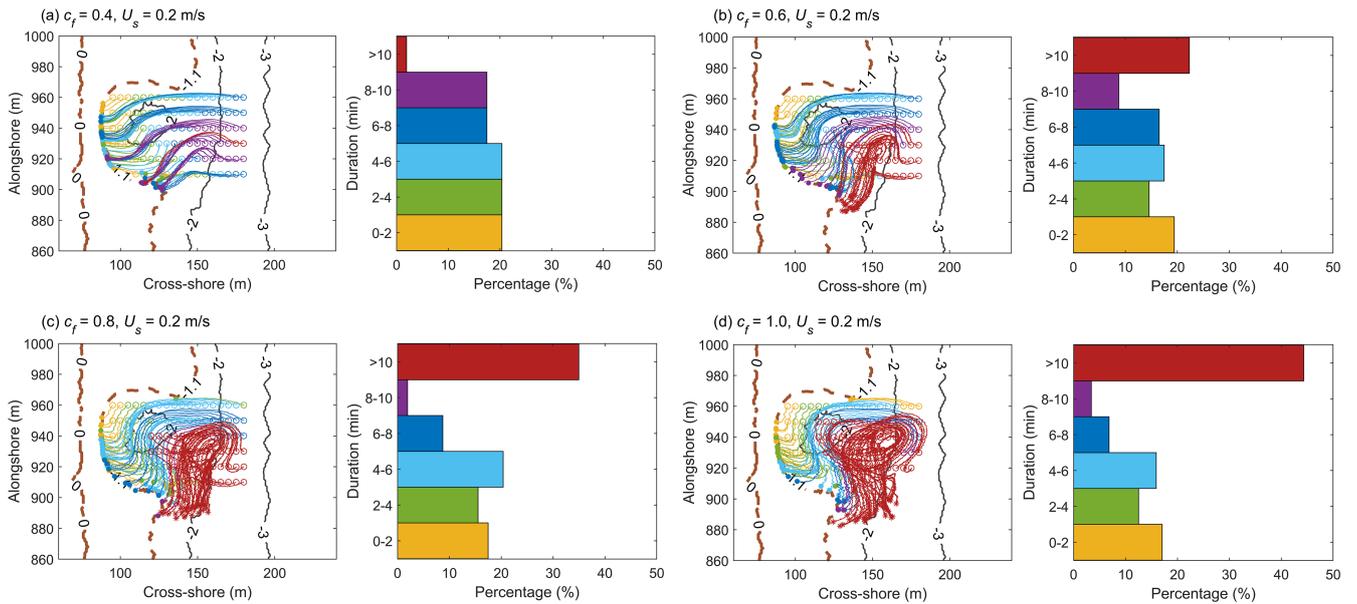
Figure 14. Sensitivity study of the floating factor c_f by varying its value from 0.4 to 1.0 with an interval of 0.2 (a-d). Swimmer tracking simulations for strategy of *swimming onshore* within Area 1 are listed in the left of each subplot, and histograms of t_{safe} are in the right. Virtual swimmers have a constant onshore swimming velocity of 0.2 m/s.